Electronic Supplementary Information

Paper-Based Photoelectrochemical Immunosensing Based on CdS QDs Sensitized Multidimensional Porous ZnO spheres Promoted by Carbon Nanotubes

Panpan Wang, Guoqiang Sun, Lei Ge, Shenguang Ge, Xianrang Song, Mei Yan, Jinghua Yu*

Reagents

Mouse monoclonal capture CEA antibodies (Ab and CEA standard solutions (0.5 $mg \cdot mL^{-1}$) were purchased from Shanghai Linc-Bio Science Co. Ltd. Blocking buffer for the residual reactive sites on the Ab immobilized PWE was phosphate buffer solution (PBS) containing 0.5% bovine serum albumin (BSA) and 0.5% casein. Tween-20 (0.05%) was spiked into 0.01 M PBS (pH 7.4) as a washing buffer to minimize unspecific adsorption. Whatman chromatography paper #1 was purchased from GE Healthcare Worldwide and used with further adjustment of size (A4 size). The aqueous solutions unless indicated were prepared with Milli-Q water (Millipore, USA). Zinc nitrate hexahy-drate ($Zn(NO_3)_2 \cdot 6H_2O$, Sinopharm Chemical Reagent Co. Ltd., Shanghai, China), ammonia hydroxide (28 wt% NH_3 in water, Sinopharm Chemical Reagent Co. Ltd.) , and starch powders (Shanghai Shiyi Chemicals Reagent Co. Ltd., Shanghai, China) used in the experiments were of analytical purity and were used without further purification. CdS NPs (5.5 nm) were prepared in water [1]. CNTs

were purchased from Nanoport. Co. Ltd. Sodium sulfide (Na_2S), cadmium acetate ($(CH_3COO)_2Cd{\cdot}3H_2O$), thiourea ($(NH_2)_2CS$) and ethylenediamine ($NH_2(CH_2)_2NH_2$) were obtained from Sigma-Aldrich Chemical Co. (St. Louis, MO). N-(3-dimethyl-aminopropyl)-N-ethylcarbodiimide (EDC), N-hydroxysuccin-imide (NHS, 98%) and poly(dimethyldiallylammonium chloride) (PDDA) (20%, w/w in water, molecular weight = 200000-350 000) were bought from Alfa Aesar China Ltd. Serum specimens from healthy persons and clinically diagnosed patients were provided by the Cancer Research Center of Shandong Tumor Hospital, and measured by the same procedure applied for CEA detection above. In order to cover the wide linear detection range of the proposed protocol, these serum samples were used either as-received or diluted to a specific concentration with 10 mM phosphate buffer solution, pH 7.4.

Apparatus

Ultrasonic processing was performed on a JY92-IIDN ultrasonic apparatus (Ningbo Scientz biotechnology Co. Ltd, China). Scanning electron microscope (SEM) analyses were performed using a QUANTA FEG-250 thermal field emission scanning electron microscopy (FEI Co., USA), and the microscope was equipped with an Oxford X-MAX50 energy dispersive spectrometer (EDS) (Oxford, Britain). Transmission electron microscope (TEM) images were obtained from a JEOL JEM-1400 microscope (JEOL, Japan). Powder X-ray diffraction (XRD) patterns were collected on a Pa D8 advance diffractometer system equipped with Cu Kα radiation (Bruker Co., Germany). Electrochemical impedance spectra (EIS) were performed on

a CHI 604D electrochemical workstation (Shanghai CH Instruments Inc., China).

Photoelectrochemical measurements were carried out with a homemade PEC system. A 500 W Xe lamp was used as the irradiation source with the light intensity about 400 $\mu W \cdot cm^{-2}$ estimated with a radiometer (Photoelectric Instrument Factory of Beijing Normal University). The photocurrent was measured on a CHI 660D electrochemical workstation (Shanghai Chenhua Apparatus Corporation, China) with a three-electrode system, whereas the modified PWE with a diameter of 6.0 mm was used as the working electrode, screen-printed carbon electrode and Ag/AgCl electrode were used as the counter electrode and the reference electrode, respectively. All PEC detection was carried out at a constant potential of 0 V in PBS (pH 7.4, 0.1 M) containing AA (0.1 M), which was deaerated by highly pure nitrogen for 15 min prior to any measurements and then kept under a N_2 atmosphere for the entire experimental process.

Design and Fabrication of μ-PECOD

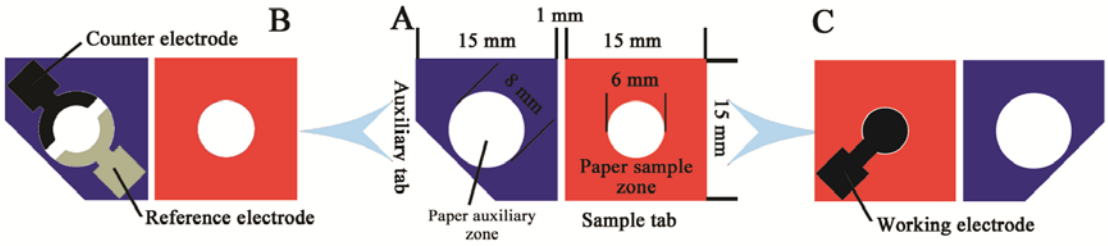

Scheme S1. (A) The schematic representation, size, and shape of this μ-PECOD. (B) One side of the μ-PECOD with the screen-printed reference and counter electrode; (C) The reverse side of (B) with the screen-printed working electrode;

The preparation of this μ-PECOD was similarly to our previous work [2] with large modifications and a detailed procedure was described below. As shown in Scheme S1A, this origami device was comprised of a square auxiliary tab (15.0 mm × 15.0 mm) and a square sample tab (15.0 mm × 15.0 mm). An angle of the square auxiliary

tab was cut off for exposure of the contact pad of screen-printed carbon working electrode (Scheme S2). The entire origami device could be produced in bulk on an A4 paper sheet by a commercially available solid-wax printer (Xerox Phaser 8560N color printer). Owing to the porous structure of paper, the melted wax can penetrate into the paper network to decrease the hydrophilicity of paper remarkably while the unprinted area (paper auxiliary zone and paper sample zone) still maintained good hydrophilicity, flexibility, and porous structure and will not affect the further screen-printing of electrodes and modifications [3].

Between the sample tab and auxiliary tab, the unprinted line (1 mm in width) was defined as fold line (Scheme S1A). The unprinted hydrophilic area (paper auxiliary zone and paper sample zone) constituted the reservoir of the paper PEC cell (~40 μL) after being folded at the predefined fold line. Then, the wax-penetrated paper sheet was ready for screen-printing of electrode containing the wire and contact pad on its corresponding paper zone (Scheme S1B, C). The electrode array consisted of a screen-printed Ag/AgCl reference electrode and carbon counter electrode on the auxiliary zone (Scheme S1B) and screen-printed carbon working electrode (6 mm in diameter) on the reverse side of paper sample zone (Scheme S1C), respectively. After folding, the three screen-printed electrodes will be connected once the paper PEC cell was filled with solution.

Synthesis of MDP ZnO Spheres.

In a typical preparation, 5 g of soluble starch was dissolved in 150 mL of boiling deionized water. Then, 0.01 mol of $Zn(NO_3)_2 \cdot 6H_2O$ was added to the resulting clear

starch solution, and the mixture was stirred at 85 °C for 5 min. The pH of the mixture solution was then adjusted to 8-9 by gradual addition of ammonium hydroxide (ca. 3 mL), and a milklike solution was formed. The solution was stirred for an additional 30 min at 85 °C, and the resulting precipitate was centrifuged, washed with deionized water, and dried at 50 °C. Then, the as-obtained powders were calcined in air atmosphere at 500 °C for 2 h to obtain MDP ZnO spheres.

Preparation of CdS QDs coated MDP ZnO Spheres

CdS/ZnO nanocomposites were prepared according to the following procedure, as reported previously with some modifications[5]. MDP ZnO spheres were first immersed in the solution of 0.1 M of Na_2S dissolved in 20 mL of deionized water and kept for 10 min at room temperature. A thin ZnS layer was then obtained on the surface of ZnO spheres, which serves as a leading layer for the formation of CdS shell layer. The sample was further immersed in the solution containing 0.025 M cadmium acetate, 0.1 M thiourea, and 0.1 M ethylenediamine for 1 h at room temperature to prepare CdS/ZnO nanocomposites. After that, 150 μL thioglycollic acid was added in the solution to react for 240 min. Then, the surface ligand (thiourea) on the as prepared CdS/ZnO nanocomposites was changed to thioglycollic acid through ligand exchange reaction.

To confirm the complete ligand exchange reaction, five ligand exchange reaction experiments were carried out simultaneously under the identical conditions for 60 min, 120 min, 180 min, 240 min, and 300 min, respectively. Then, the resulting thioglycollic acid-capped CdS/ZnO composites were centrifuged, washed, and

suspended in PBS solution (pH 7.4). These CdS/ZnO composites with different amount of surface ligands (thioglycollic acid) were employed to construct the Ab/CdS/ZnO/PDDA-CNTs/PWE under the identical conditions. Then, the EIS of these obtained Ab/CdS/ZnO/PDDA-CNTs/PWEs were carried out in a background solution of 10 mM $[Fe(CN)_6]^{3-/4-}$ containing 0.5 M KCl at a bias potential of 170 mV (versus Ag/AgCl). As shown in Fig. S1, the electron-transfer resistance of the modified PWEs increased with the increasing of the ligand exchange reaction time and then reached its maximum value at 240 min, indicated that no more Ab was immobilized in the CdS/ZnO/PDDA-CNTs/PWEs for longer ligand exchange reaction time (>240 min), which confirm that the complete ligand exchange reaction could be achieved at 240 min.

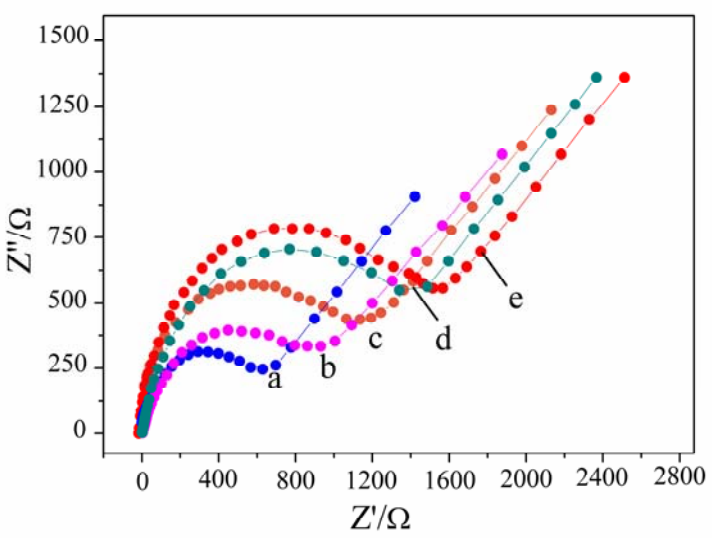

Fig. S1. EIS of the Ab/CdS/ZnO/PDDA-CNTs/PWE with different amount of thioglycollic acid on the surface of CdS/ZnO. The ligand exchange reaction time: (a) 60 min; (b) 120 min; (c) 180min; (d) 240 min; (e) 300 min.

Fig. S2A and B displays the SEM and TEM images of the ZnO samples calcined at 500 °C in air for 2 h. It indicates that the diameters of the ZnO spheres is about 150-400 nm after calcination for the removal of soluble starch and the aggregation of

the nanoparticles. A single MDP ZnO spheres results from the agglomeration of crystalline subcrystals ranging from 20 to 45 nm and owns the rough surface. The starch granules swell and burst in boiling water, and the semicrystalline structure is lost as the smaller amylose molecules start leaching out of the granule. It is likely that the majority of the zinc ions are closely associated with the starch molecules, so nucleation and initial crystal growth might preferentially occur within regions of both high starch concentration and high Zn^{2+} concentration [7]. In most cases, the van der Waals interactions between the surface molecules of the nanocrystallites form the driving force for self-assembly, and then ZnO nanocrystals can be assembled to form larger ZnO spheres. This MDP structure provides continuously conductive pathways for the transportation of photoinduced electrons and its high specific surface area is beneficial for adsorption of CdS QDs. Comparing with Fig. S2A and Fig. S2C, we can see that the surface texture of ZnO spheres changed after CdS QDs were bonded to ZnO spheres. What's more, EDS analysis of CdS/ZnO nanocomposite was performed to further demonstrate the successful combination. It was observed that the elements Cd and S existed in site "1" from Fig. S2C.

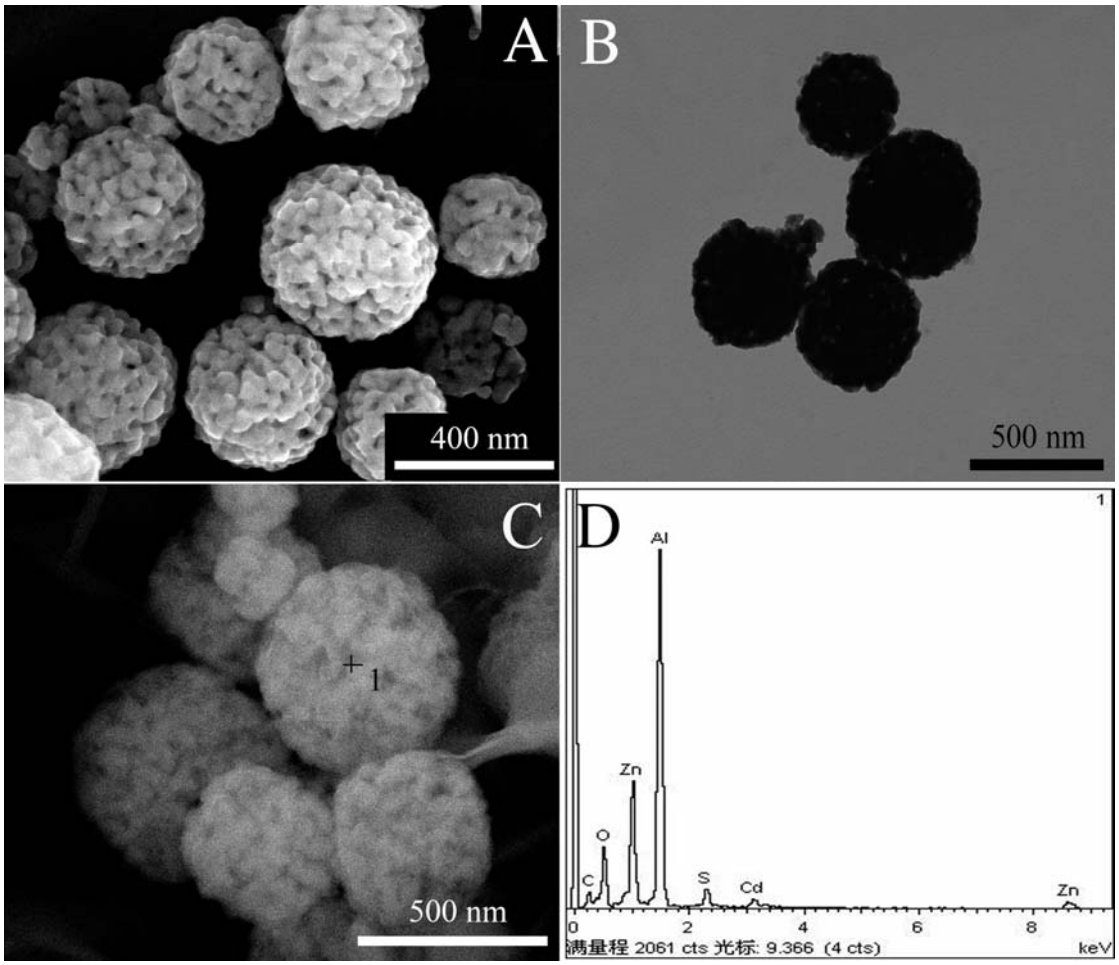

Fig. S2. SEM (A) and TEM (B) images of the ZnO powders obtained after calcination at 500 °C for 2 h; (C) SEM image of the CdS/ZnO nanocomposites; (D) EDS of CdS/ZnO nanocomposites.

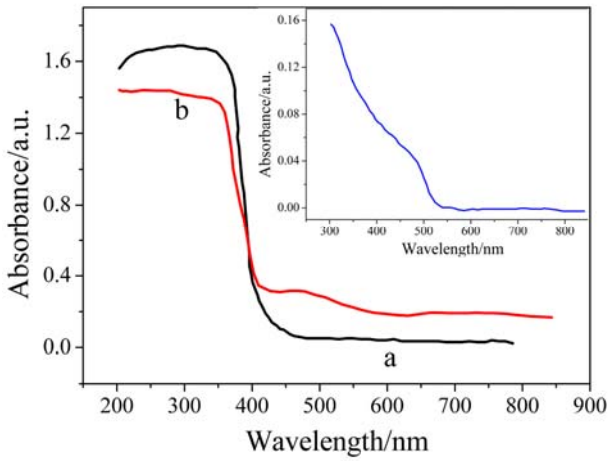

Fig. S3. The linear optical absorption properties of (a) pure ZnO film and (b) CdS/ZnO composite film. The inset shows the optical spectrum of pure CdS QDs dispersed in ethanol solution.

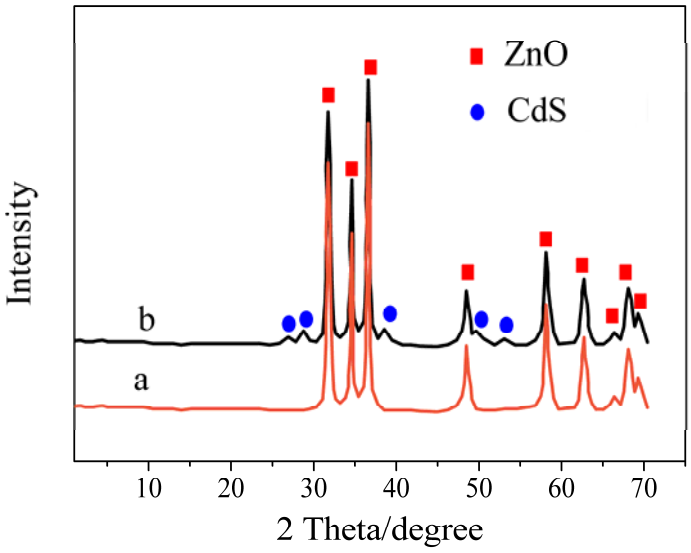

Fig. S4. XRD patterns of the (a) ZnO spheres calcined at 500 °C for 2 h and (b) CdS/ZnO nanocomposites.

From Fig. S4, all of the diffraction peaks of the calcined powders match well with those of the standard ZnO XRD pattern (JCPDS 89-7102) and are attributed to the wurtzite phase. In contrast to the XRD pattern of ZnO, the CdS/ZnO nanocomposites show five more peaks, which are ascribed to the crystal planes of CdS NPs, further confirm that the CdS NPs on the surface of ZnO are of hexagonal structure (JCPDS 06-0314). These results demonstrated the single-crystal quality of the CdS NPs on the ZnO spheres, which made the diffraction peaks of the CdS sharp and well identified.

Construction of Ab/CdS/ZnO/PDDA-CNTs/PWE

Firstly, PDDA-CNTs were prepared according to the following procedure, as reported previously with some modifications [5]. CNTs were first sonicated with 3:1 (v/v) H_2SO_4/HNO_3 for 4 h to obtain carboxylic group-functionalized CNTs. The resulting dispersion was filtered and washed repeatedly with water until the pH was

about 7.0. Then 0.5 $mg \cdot mL^{-1}$ CNTs were dispersed into a 0.25% PDDA aqueous solution containing 0.5 M NaCl and the resulting dispersion was sonicated for 30 min to give a homogeneous black suspension. Residual PDDA was removed by centrifugation, and the complex was rinsed with water. The collected complex was redispersed in water with mild sonicating.

The PWEs on the PEC reaction disc were firstly modified through sequentially assembling positively charged PDDA-CNTs and negative charged CdS/ZnO nanocomposites onto the surfaces of interwoven cellulose fibers in paper sample zones. Briefly, 20 μL solution of PDDA-CNTs and 20 μL solution of CdS/ZnO nanocomposites were alternately dropped into the paper sample zone and kept it for 10 min. After each dropping step, the paper sample zone was rinsed thoroughly according to the method demonstrated in our previous work [6]. Then, a fresh prepared 15 μL solution of EDC (10 $mg \cdot mL^{-1}$) and of NHS (20 $mg \cdot mL^{-1}$) were added into the CdS/ZnO/PDDA-CNTs/PWE to active the CdS NPs for 35 min followed by washing thoroughly with water, then 20 μL of 20 $\mu g \cdot mL^{-1}$ Ab solution was dropped into the activated PWE and the PEC reaction disc was then incubated at 4 °C for 4 h. Subsequently, physically absorbed excess Ab was rinsed with phosphate buffer solution (PBS, pH 7.4). Finally, the Ab/CdS/ZnO/PDDA-CNTs/PWE was blocked by the blocking buffer for 0.5 h to cover the possible remaining active sites.

In the paper, CEA/BSA/Ab/ZnO/PDDA-CNTs/PWE was fabricated according to our previous work [6]. CEA/BSA/Ab/CdS/PDDA-CNTs/PWE was fabricated in the same procedure as CEA/BSA/Ab/CdS/ZnO/PDDA-CNTs/PWE.

Characterization of Ab/CdS/ZnO/PDDA-CNTs/PWE

Prior to the immobilization of CdS/ZnO nanocomposites into the paper sample zone of PWE, PDDA-CNTs was assembled onto the surfaces of interwoven cellulose fibers through electrostatic interactions to enhance the conductivity of paper sample zone and enlarge the effective surface area of PWE. The morphologies of PDDA-CNTs modified paper sample zones were characterized by SEM. Fig. S5A showed that the nano-scale interconnected PDDA-CNTs were firmly entangled on micro-scale cellulose fibers in the form of small bundles or single tubes. Then, CdS/ZnO nanocomposites were connected to the surface of the PDDA-CNTs/PWE (Fig. S5B) to greatly increase the active surface area, which enhanced the effective absorption of photons.

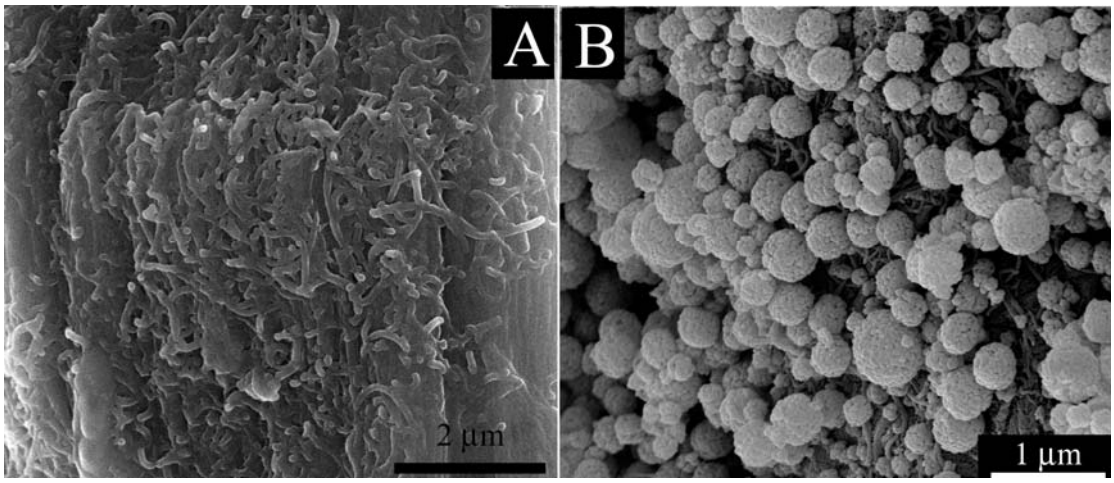

Fig. S5 (A) SEM image of PDDA-CNTs entangled cellulose fibers in paper sample zone; (B) SEM image of CdS/ZnO/PDDA-CNTs fabricated paper sample zone.

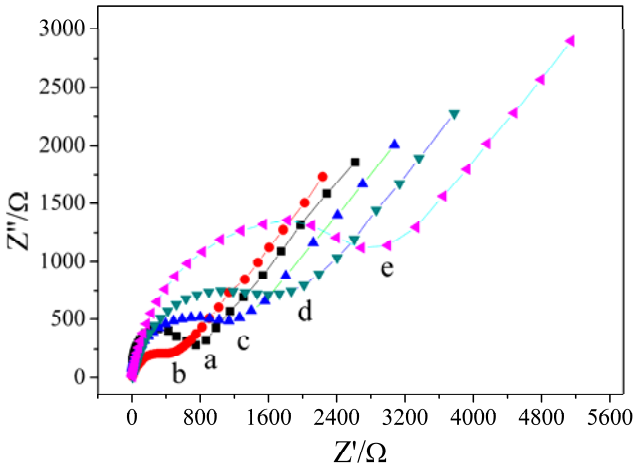

Fig. S6. EIS of the PWE under different condition in 10.0 mM $[Fe(CN)_6]^{3-/4-}$ solution containing 0.5 M KCl: (a) bare PWE; (b) PDDA-CNTs/PWE; (c) CdS/ZnO/PDDA-CNTs/PWE; (d) Ab/CdS/ZnO/PDDA-CNTs/PWE; (e) Ab/CdS/ZnO/PDDA-CNTs/PWE after blocking.

As shown in Fig. S6, the bare PWE showed a relatively small electron-transfer resistance, R_{et} (curve a). After PDDA-CNTs was formed on the cellulose fiber surface in paper sample zone, a much smaller R_{et} was observed (curve b) while the anchoring of CdS/ZnO NPs showed a much larger R_{et} (curve c). The reason may be that the PDDA-CNTs immobilized on the cellulose fiber surfaces played an important role similar to a conducting wire, which provided a fast electron transfer path to the PWE, while the assembly of CdS/ZnO nanocomposites into the PDDA-CNTs/PWE partially blocked the electron transfer of the redox probe. Remarkable increase in the R_{et} value was observed after both the immobilization of Ab (curve d) and blocking with BSA (curve e) on the surfaces of CdS/ZnO/PDDA-CNTs modified cellulose fibers in PWE, indicating that the electron-transfer kinetics of the redox probe was slow down, which testified the successful immobilization of Ab and BSA blocking.

PEC assay procedures of this μ-PECOD

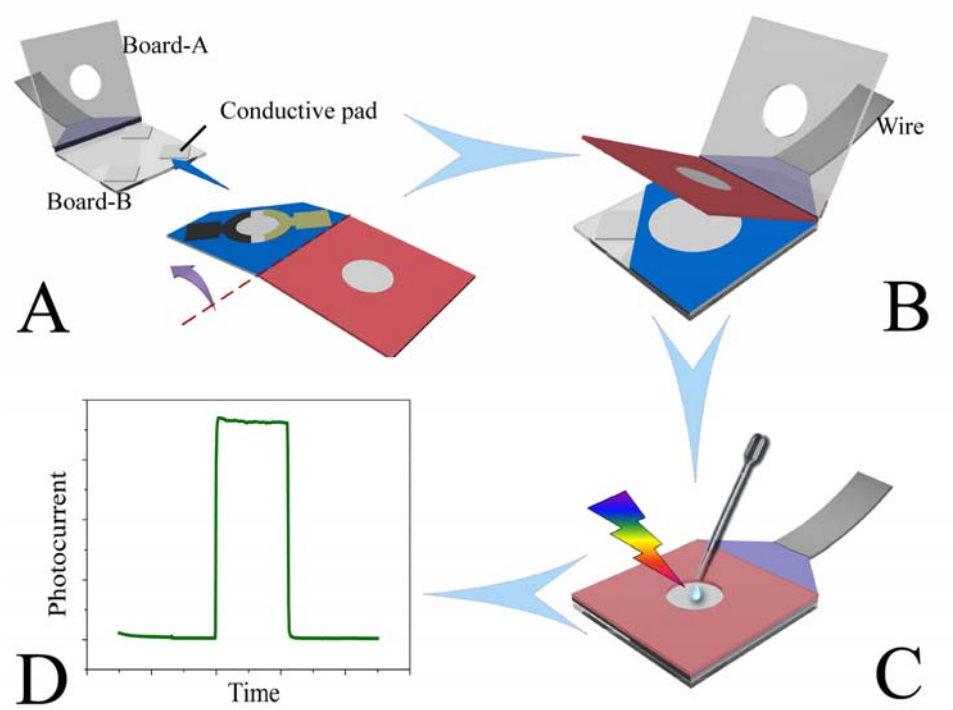

Scheme S2. Schematic representation of the assay procedures for this μ-PECOD: (A) The auxiliary tab was folded down below the sample tab; (B) The μ-PECOD was clamped into the device holder; (C) visible light and AA were used to trigger the PEC reaction; (D) PEC response of the μ-PECOD with visible light irradiation.

The PEC assay procedures on μ-PECOD were shown in Scheme 1A and Scheme S2, and a detailed procedure was described as below: First, 25 μL of analyte (CEA) solution with different concentrations were added and the mixture was incubated at 37 °C for 240 s followed by washing with the washing buffer solution four times. Then, the auxiliary tab was folded down below the sample tab and clamped with a home-made device-holder similar to our previous work [2], which was comprised of two circuit boards (named Board-A and Board-B respectively below) with conductive pads on them, to fix and connect this origami device to the electrochemical workstation (Shanghai CH Instruments Co., China) as shown in Scheme S2A. Finally,

a 40 μL PBS containing 0.1 M AA were applied into the paper PEC cell through the hole on Board-A (Scheme S2C). Under visible light irradiation, photocurrent signal was obtained.

Condition Optimization

To optimize the experimental condition for CEA measurement, the effects of applied potential, the excitation wavelength, incubation temperature and time for the antibody-antigen interaction were investigated. Applied potential is an important factor relevant to the photocurrent response. As seen in Fig. S7A, upon addition of 0.1 M AA, with an increase of potential from -0.3 V to 0 V, the photocurrent increases sharply. A negative potential can inhibit the electron transfer from CdS/ZnO to the electrode, which may lead to the electron hole recombination. In the potential range from 0 to 0.3 V, the photocurrent sharply improved. However, the photocurrent at 0 mV shows acceptable sensitivity for the PEC detection of CEA. The low applied potential was beneficial to the elimination of interference from other reductive species that coexisted in the real samples. Therefore, 0 V was selected as the applied potential for the determination of CEA.

The irradiation wavelength is another significant factor that is relevant to the photocurrent response. As shown in Fig. S7B, upon addition of 0.1 M AA, the photocurrent increased as the exciting wavelength increased from 420 nm to 470 nm at the applied potential of 0 V. Afterward, the photocurrent quickly decreased. Moreover, considering that biomolecules may suffer from irradiation with light of excessively short wavelength. Thus, 470 nm was chosen for the PEC biosensing of

CEA.

Fig. S7C shows the effect of incubation temperature on the photocurrent responses for the CEA, which was examined at different temperatures ranging from 25 to 50 °C. The photocurrent responses increased with increasing temperature up to 37 °C, which is attributed to the increasing immunoreaction rate between anti-CEA antibodies and CEA. However, when temperature was over 37 °C, the photocurrent response decreased. The reason may be that the high temperature caused an irreversible denaturation of proteins. In addition, temperatures lower than 37 °C could reduce the immunoreaction rate; thus the incubation time should be prolonged. In the following experiments, 37 °C was employed as the optimal incubation temperature for further studies.

As shown in Fig. S7D, the photocurrent responses decreased with incubation time and reached a plateau at 240 s. An incubation time longer than 240 s did not sharply reduce the response. Consequently, 240 s was chosen as the incubation time for determination of CEA. The incubation process on this μ-PECOD needed shorter time compared with 40-120 min at 37 °C for the traditional PEC immunoassay. This is partly due to the high surface-to-volume ratio, incompact porous structure, and the small volume of the PDDA-CNTs modified paper sample zone. The immunoreagents diffused only short distances to react with each other. Furthermore, as the solutions dry in the paper zones, the concentration of each reagent increases; this concentration maybe further enhances the binding kinetics of antibody-antigen [8]. Finally, the short incubation times could be favorable to high sample throughput and rapid point-of-care

testing.

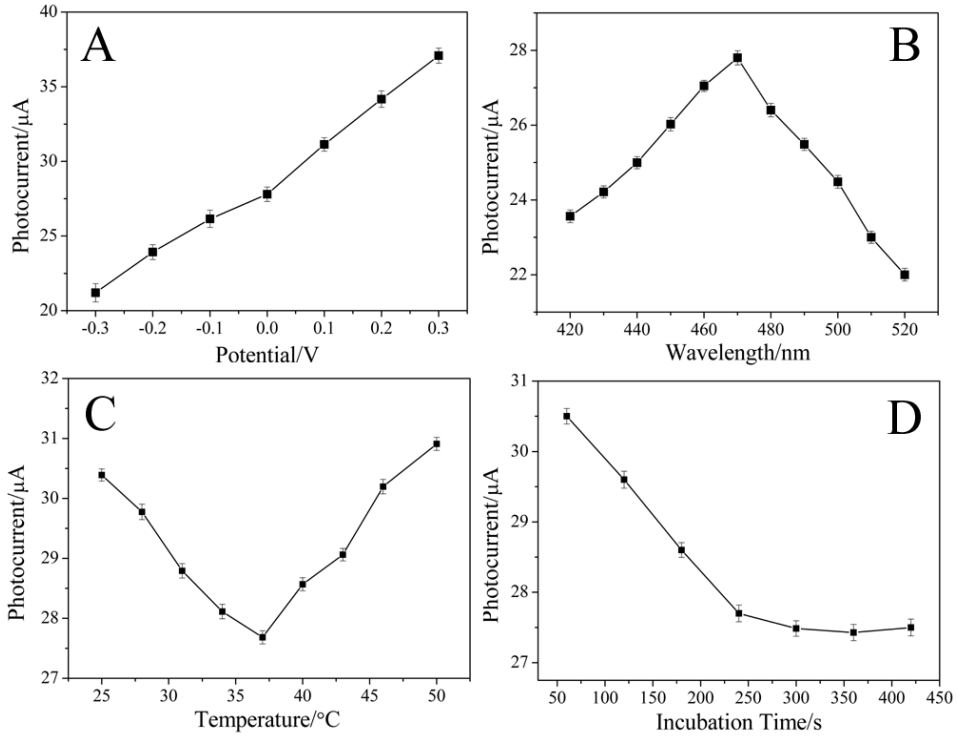

Fig. S7. Effects of (A) applied potential, (B) excitation wavelength, (C) incubation temperature and (D) incubation time on photocurrent responses of CdS/ZnO/PDDA-CNTs/PWE in 0.1 M pH 7.4 PBS containing 0.1 M AA after incubated in CEA solution.

Reproducibility, Specificity and Stability of this μ-PECOD immunosensor

The reproducibility of an assay was expressed in terms of values for a within-batch (intra-assay) and a between-batch (interassay) relative standard deviation (RSD). Analyzed from the experimental results, the intra-assay RSDs were 5.8%, 4.2%, and 3.7% at CEA concentrations of 0.02, 0.1, and 1.5 ng·mL^{-1}, respectively. The interassay RSDs of 3.1%, 3.5%, and 2.8% were obtained by measuring the same samples with eleven μ-PECODs prepared independently under identical experimental conditions. The results indicated a satisfactory precision and reproducibility of the proposed protocol.

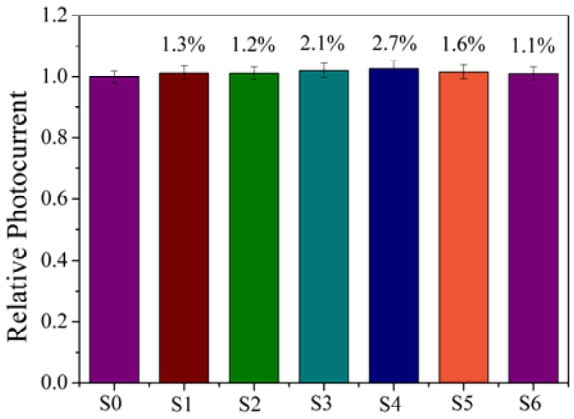

Fig. S8. Relative photocurrent in different mixture systems on CEA sensor for 5 ng·mL^{-1} CEA only (S0), 5 ng·mL^{-1} CEA + 50 ng·mL^{-1} AFP (S1), 5 ng·mL^{-1} CEA + 50 ng·mL^{-1} PSA (S2), 5 ng·mL^{-1} CEA + 50 ng·mL^{-1} CA125 (S3), 5 ng·mL^{-1} CEA + 50 ng·mL^{-1} HSA (S4), 5 ng·mL^{-1} CEA + 50 ng·mL^{-1} HIgG (S5), mixed sample (S6). (Five measurements for each point).

Usually, nonspecific adsorption is a major problem in immunosensing, since it cannot be distinguished from specific adsorption and consequently influences the sensitivity. In order to prove that the as-observed photocurrent changes arise from specific interaction between the antibody and the antigen, controllable experiments were performed. The photocurrent responses of BSA-blocked PWE in the presence of a mixture containing 5 ng·mL^{-1} CEA without or with 50 ng·mL^{-1} α-fetoprotein (AFP), prostatespecific antigen (PSA), carcinoma antigen 125 (CA125), human serum albumin (HSA), and human IgG (HIgG) are shown in Fig. S8. As can be seen, compared to the result obtained in the presence of only CEA, no significant photocurrent differences were found with the single interfering protein, although its concentration is 10 times of that of CEA. The specificity of the proposed protocol was further evaluated by measuring the photocurrent response of mixture containing 5

ng·mL^{-1} CEA, and 50 ng·mL^{-1} AFP, PSA, CA125, HSA and HIgG. No obvious photocurrent difference could be observed when the mixed sample contained four different interfering proteins and each concentration was 10-fold that of CEA. All these results demonstrate that the observed photocurrent is mainly due to the specific binding without obvious interference from nonspecific adsorption.

The long-term stability of the competitive immunosensor was also examined. When the μ-PECOD was stored in a dark and moisturizing environment at 4 °C over 2 weeks, no apparent change in photocurrent response for the detection of CEA was found, illustrating its good long-term storage stability.

As shown in Table S1, by comparison with the ELISA method, the RSDs obtained from the developed method showed acceptable feasibility to detect CEA in human serum. These two results were in good agreement, demonstrating that the developed immunosensor with high sensitivity, selectivity, and stability has a potential application in clinical diagnosis in future.

Table S1. Comparison Assay Results of Clinical Serum Samples for ELISA and the Proposed Method

Serum sample	ELISA (ng·mL^{-1})	Proposed method (ng·mL^{-1})	Rel deviation (%)
1	0.0200	0.0204	2.0
2	0.0500	0.0491	-1.8
3	0.150	0.155	3.3
4	0.511	0.501	-1.96
5	1.39	1.40	1.44
6	2.26	2.24	-0.88
7	3.56	3.54	-0.56

Table S2. Comparison of the linear range and detection limit using different methods

analyte	measurement protocol	limit of detection, linear range	ref
CEA	Flow injection electrochemical	0.5 to 25 ng·mL^{-1}, 0.22 ng·mL^{-1}	9
CEA	Electrochemical	0.16 to 9.2 ng·mL^{-1}, 0.04 ng·mL^{-1}	10
CEA	Chemiluminescent	1.0 to 70 ng·L^{-1}, 0.65 ng·mL^{-1}	11
AFP	TiO_2-CdS-PEC	0.05 to 50 ng·mL^{-1}, 40 pg·mL^{-1}	12
α-Synuclein	TiO_2-Au-PEC	0.05 to 100 ng·mL^{-1}, 34 pg·mL^{-1}	13
CEA	CdS/ZnO/PDDA-CNTs/PEC	0.01 to 50 ng·mL^{-1}, 4 pg·mL^{-1}	This work

Reference

1. G.-L. Wang, P.-P. Yu, J.-J. Xu and H.-Y. Chen *J. Phys. Chem. C* , 2009, **113**, 11142.
2. J. Lu, S. Ge, L. Ge, M. Yan, J. Yu, *Electrochim. Acta,* 2012, **80,** 334.
3. E.Carrilho, A. W. Martinez, G. M. Whitesides, *Anal. Chem.,* 2009, **81,** 7091.
4. L. Wang, S. Guo, L. Huang, S. Dong. *Electrochem. Commun*., 2007, **9**, 827.
5. Z. Z. Lu, J. X, H. K. Wang, C. D. Wang, S. Y. Kwok, T. Wong, H. L. Kwong, I. Bello, C. S. Lee, S. T. Lee and W. J. Zhang, *J. Phys. Chem. C* 2012, **116**, 2656.
6. J. Yan, L. Ge, X. Song, M. Yan, S. Ge, J. Yu, *Chem. Eur. J.* 2012, **18**, 4938.
7. A. Taubert, G. J. Wegner, *Mater. Chem.*, 2002, **12**, 805.
8. C.-M. Cheng, A.W. Martinez, J. Gong, C.R. Mace, S.T. Phillips, E. Carrilho, K.A. Mirica, G.M. Whitesides, *Angew. Chem. Int. Ed.*, 2010, **49**, 4771.
9. J. Wu, J. H. Tang, Z. Dai, F. Yan, H. X. Ju and N. E. Murr. *Biosens. Bioelectron.*, 2006, **22**, 102.
10. J. Wu, Y. T. Yan, F. Yan and H. X. Ju. *Anal. Chem.*, 2008, **80**, 6072.
11. Z. F. Fu, Z. J. Yang, J. H. Tang, H. Liu, F. Yan and H. X. Ju. *Anal. Chem.*, 2007, **79**, 7376.
12. G. L. Wang, J. J. Xu, H. Y. Chen and S. Z. Fu. *Biosens. Bioelectron.*, 2009, **25**, 791.
13. Y. R. An, L. L. Tang, X. L. Jiang, H. Chen, M. C. Yang, L. T. Jin, S. P. Zhang, C. G. Wang and W. Zhang. *Chem. Eur. J.* 2010, **16**, 14439.